Electronic Supplementary Material (ESI) for Dalton Transactions

fac-Re(CO)$_3$ complexes of 2,6-bis(4-substituted-1,2,3-triazole-1-ylmethyl)pyridine "click" ligands: synthesis, characterisation and photophysical properties.

Christopher B. Anderson, [a]Anastasia B. S. Elliott,[a, b] James E. M. Lewis,[a] C. John McAdam,[a] Keith C. Gordon[a, b] and James D. Crowley[a,*]

Table of Contents

Contents

Table of Contents 2

1. Stability Experiments 3

1.1 Competitive Histidine ^{1}H NMR Experiment 3

1.1.1 3a 3

1.1.2 3b 3

1.2 $[Re(CO)_3(2a)](PF_6)$ Stability at 40 °C 3

1.3 HR-ESI-MS Data: Competitive Histidine ^{1}H NMR Experiment 7

1.3.1 3a 7

1.3.2 3b 8

2. Selected ^{1}H NMR spectra of synthesized compounds. 9

3. HR-ESI-MS 14

4. X-ray Crystallography 16

5. Emission Spectroscopy 19

6. Density Functional Theory Calculations 20

7. References 22

1. Stability Experiments

1.1 Histidine Competition ^{1}H NMR Experiments

1.1.1 3a

3a (0.07 g, 8.66 µmol, 1 equiv.) was dissolved in 300 µL d_6-DMSO. To this 365 µL DL-histidine hydrochloride monohydrate 23.8 mM (d_6-DMSO) was added with an equivalent amount of $NaHCO_3$ (0.002 g, 8.66 µmol, 1.0 equiv.). The resulting solution was held at 40 °C and monitored using ^{1}H NMR. Spectra were acquired every 15 minutes for the first hour, then every 30 minutes for the next six hours followed by twice more 24 and 48 hours after the obtaining the initial ^{1}H NMR spectrum (Figure S1-1).

1.1.2 3b

d_6-DMSO (0.75 mL) was added to **3b** (0.012 g, 0.02 mmol, 1 equiv.), $NaHCO_3$ (0.002 g, 0.02 mmol, 1.0 equiv.) and DL-histidine hydrochloride monohydrate (0.004 g, 0.02 mmol, 1 equiv.) and the mixture stirred until complete dissolution had occurred. The resulting solution was held at 40 °C and monitored using ^{1}H NMR. Spectra were acquired every 15 minutes for the first hour, then every 30 minutes for the next 16 hours and subsequently at 36 hours (Figure S1-2).

1.2 $[Re(CO)_3(2a)](PF_6)$ Stability at 40 °C

A solution of **3a** in d_6-DMSO was held at 40 °C for seven days in darkness and the rate of decomposition was monitored periodically by ^{1}H NMR monitoring (Figure S1-3).

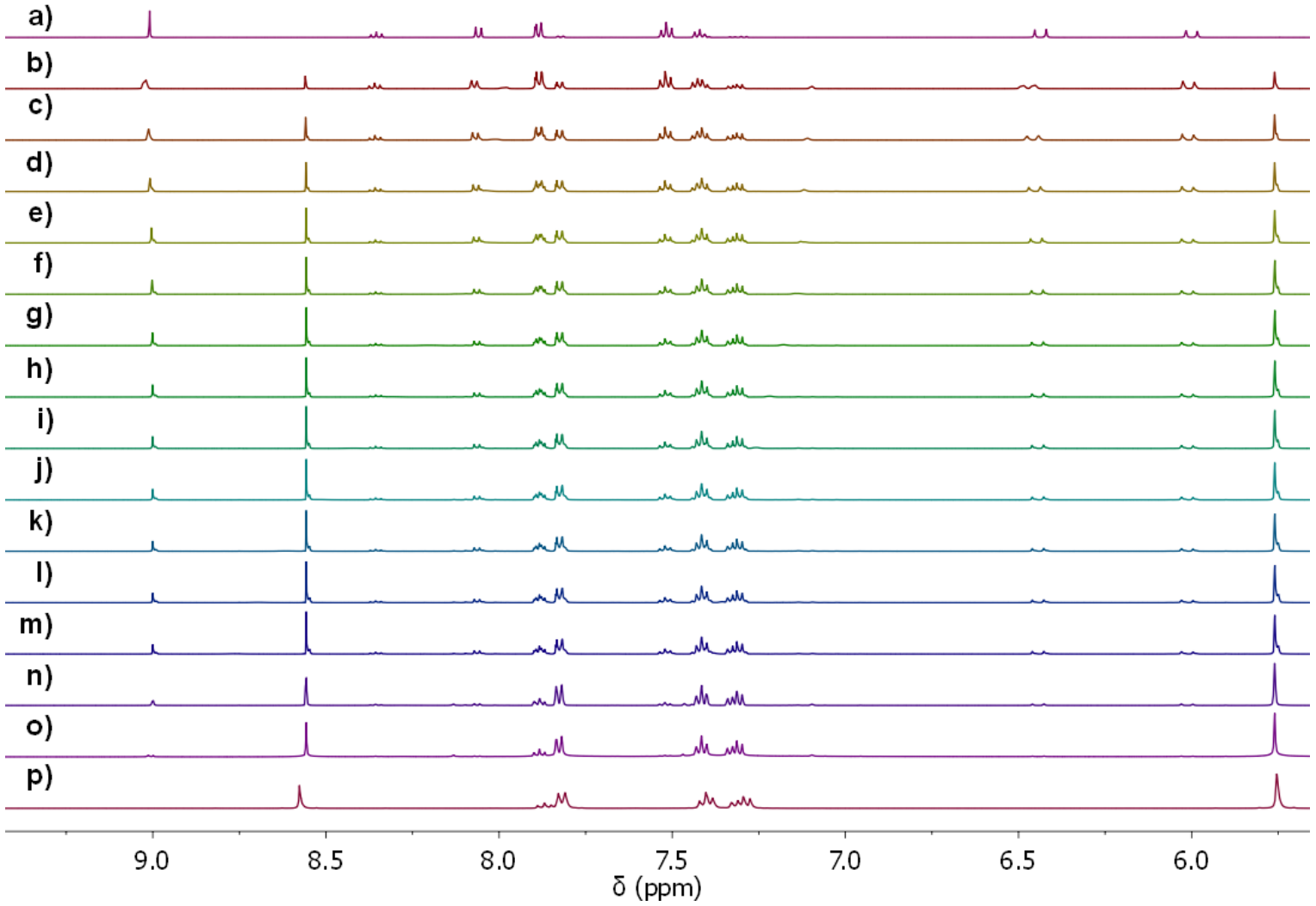

Figure S1-1 Partial ^{1}H NMR spectra (500 MHz, d_6-DMSO, 313 K) of the competitive histidine experiments showing a) the *fac*-Re(CO)$_3$ complex **3a**, and the reaction mixture with histidine after b) 15 minutes, c) 30 minutes, d) 45 minutes, e) 60 minutes, f) 90 minutes, g) 120 minutes, h) 150 minutes, i) 180 minutes, j) 210 minutes, k) 240 minutes, l) 270 minutes , m) 280 minutes, n) 24 hours, o) 48 hours, and p) the free ligand **2a**.

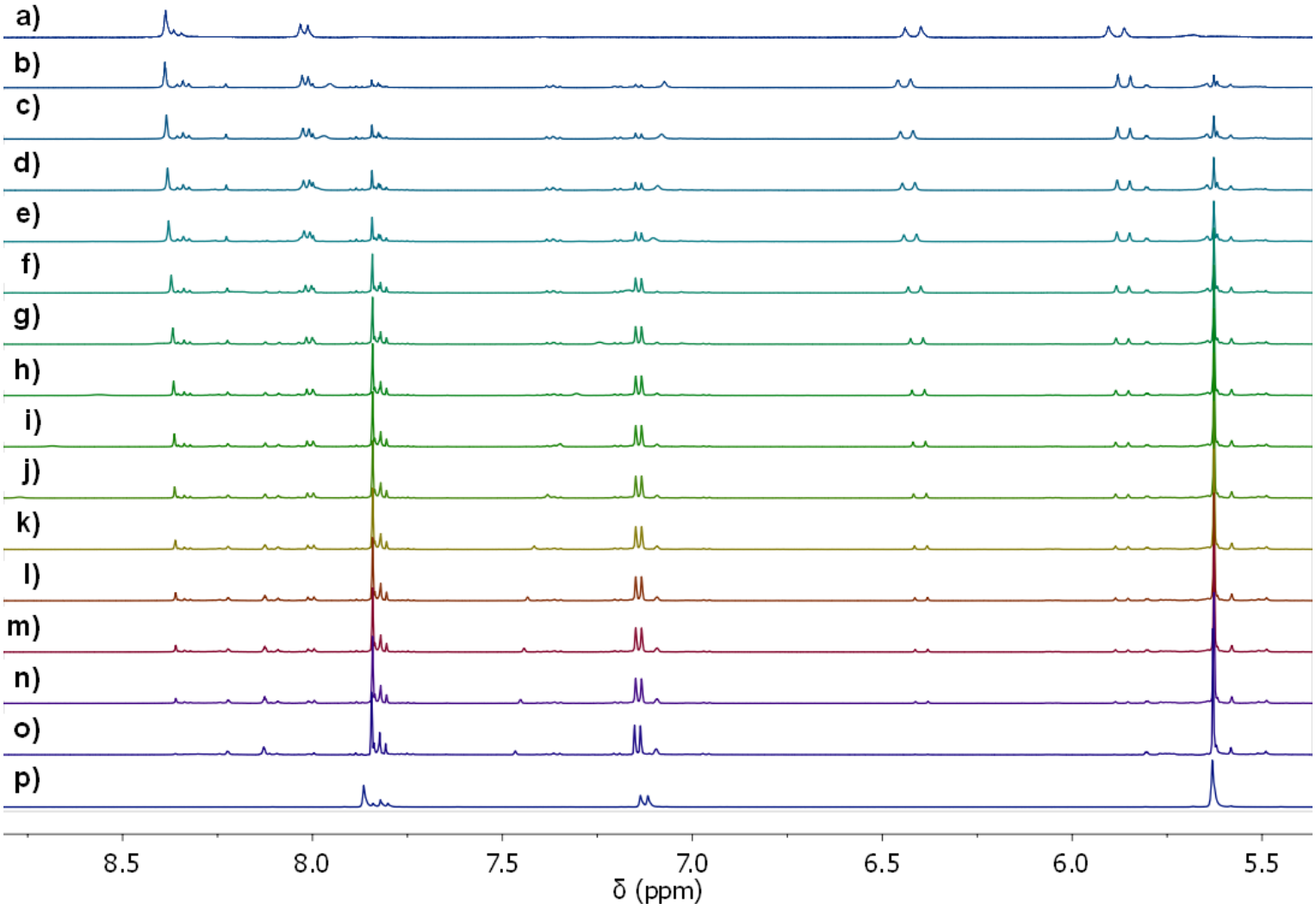

Figure S1-2 Partial ^{1}H NMR spectra (500 MHz, d_6-DMSO, 313 K) of the competitive histidine experiments showing a) the *fac*-Re(CO)$_3$ complex **3b**, and the reaction mixture with histidine after b) 15 minutes, c) 30 minutes, d) 45 minutes, e) 60 minutes, f) two hours, g) three hours, h) four hours, i) five hours, j) six hours, k) eight hours, l) ten hours, m) 12 hours, n) 16 hours, o) 36 hours, and p) the free ligand **2b**.

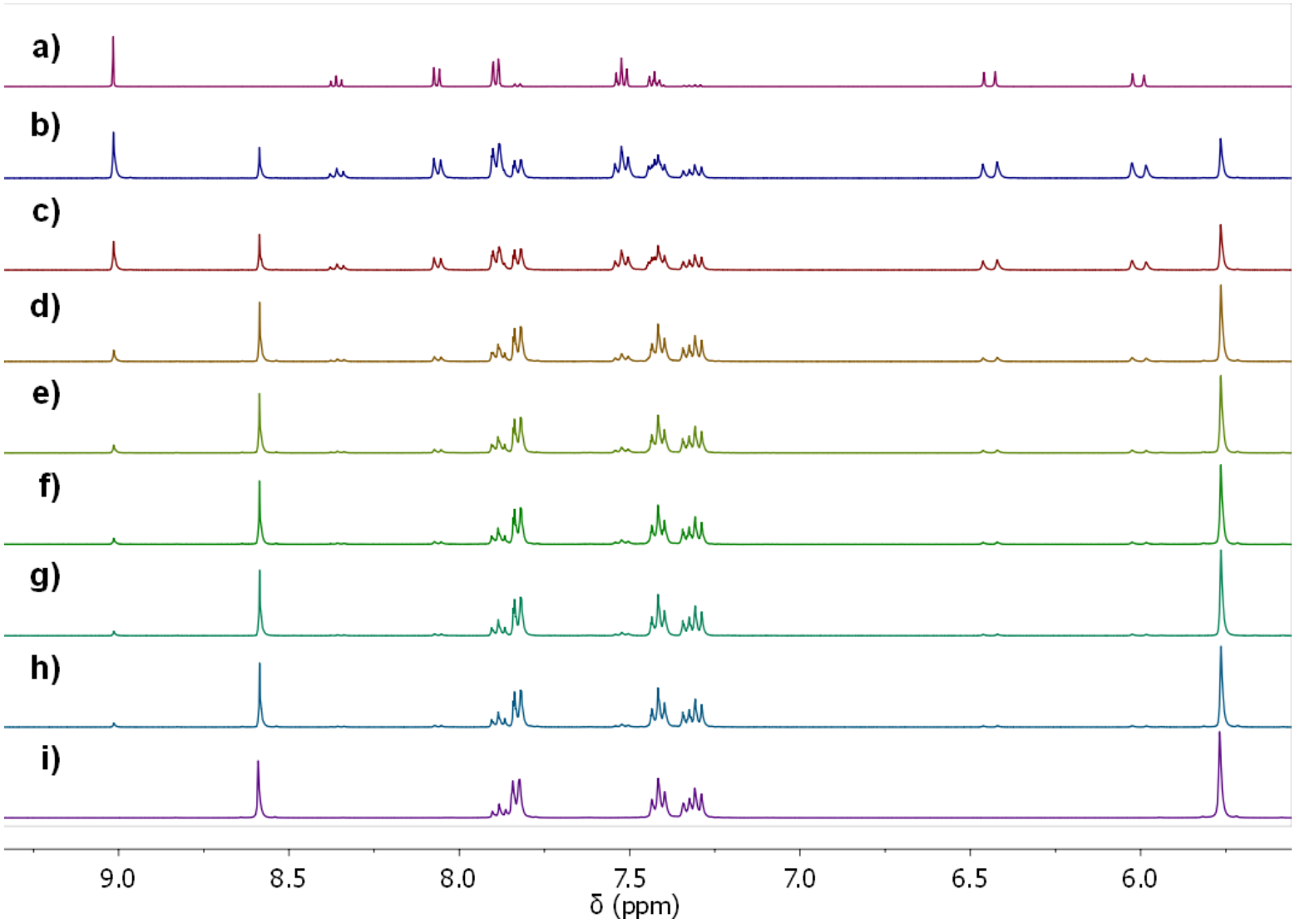

Figure S1-3 Partial ^{1}H NMR spectra (500 MHz, d_6-DMSO, 313 K) of the decomposition of **3a** at 40 °C with a) **3a** before heating, and after b) one hour, c) 18 hours, d) 91 hours, e)118 hours, f)139 hours, g) 163 hours, and h) one week heating at 40 °C, and i) free **2a**

1.3 HR-ESI-MS Data: Histidine Competition Experiment

1.3.1 3a

After the completion of the ^{1}H NMR competition experiments the d_6-DMSO reaction mixtures were analysed by ESI-MS. The spectra displayed a mixture of the following decomposition products of $[Re(CO)_3(\mathbf{2a})](PF_6)$:

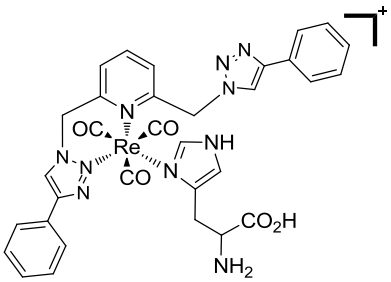

Observed: 819.1918 *m/z*
[**3a** + His]$^+$
Calc. for $C_{32}H_{28}N_{10}O_5Re$:
819.1797

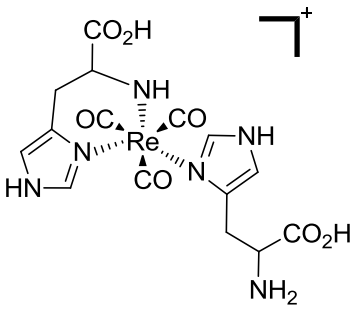

Observed: 581.0888 *m/z*
$[Re(CO)_3(His)_2]^+$
Calc. for $C_{15}H_{18}N_6O_7Re$:
581.0789

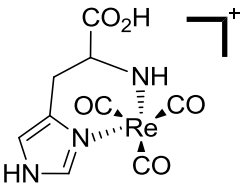

Observed: 426.0180 *m/z*
$[Re(CO)_3His]^+$
Calc. for $C_9H_9N_3O_5Re$:
426.0094

Furthermore adducts of **2a** were also detected: ESI-MS (MeOH) *m/z* = 809.3370 [(**2a**)$_2$ + Na]$^+$ (calc. for $C_{46}H_{28}N_{10}O_5Re$ 809.3296), 787.3556 [(**2a**)$_2$ + H]$^+$ (calc. for $C_{46}H_{39}N_{14}$ 787.3477), 549.2551 [**2a** + His + H]$^+$ (calc. for $C_{29}H_{28}N_{10}O_2$ 549.2469).

The peaks corresponding to [**2a + H**]$^+$ and [**3a**-PF_6]$^+$ were also detected (394.1844 and 664.1091 *m/z* respectively)

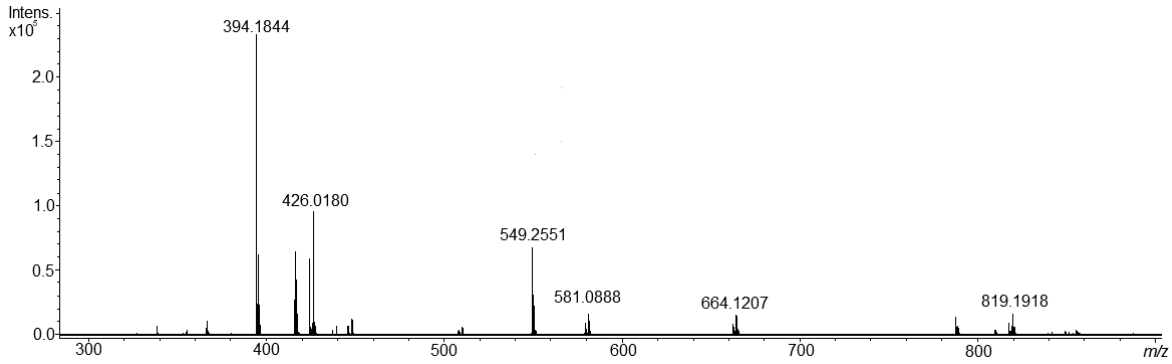

Figure S1-4 ESI-MS of the observed decomposition products highlighting some of the relevant *m/z* peaks.

1.3.2 3b

After the completion of the ^{1}H NMR competition experiments the d_6-DMSO reaction mixtures were analysed by ESI-MS.ESI-MS of the mixture following decomposition of [Re(CO)$_3$(**2b**)](PF$_6$) indicated the following Re(CO)$_3$ adduct had formed:

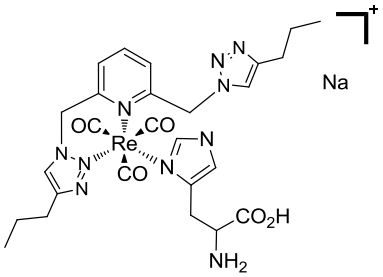

Observed: 773.1926 *m/z*
[**3a** + His + Na]$^+$
Calc. for $C_{26}H_{31}N_{10}NaO_5Re$: 773.1934

Furthermore the histidine adduct of **2b** was also detected: ESI-MS (MeOH) *m/z* = 673.3934 [(**2b**)$_2$ + Na]$^+$ (calc. for $C_{34}H_{46}N_{14}Na$ 673.3934),

The peaks corresponding to [**2b** + H]$^+$, [**2b** + Na]$^+$ and [**3b-PF$_6$**]$^+$ were also detected (326.2015, 348.1917 and 596.1420 *m/z* respectively)

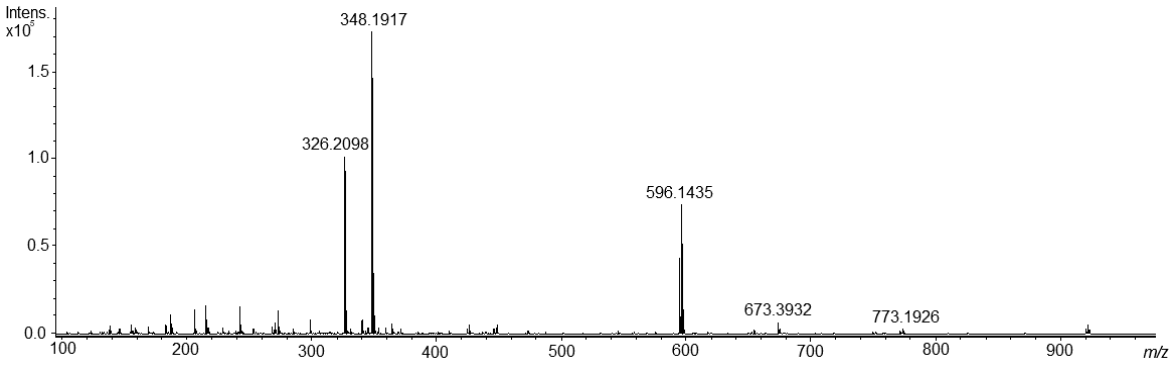

Figure S1-5 ESI-MS of the observed decomposition products highlighting some of the relevant *m/z* peaks.

2. Selected ^{1}H NMR spectra of synthesized compounds.

^{1}H NMR (d_6-acetone, 300K) of **2b.**

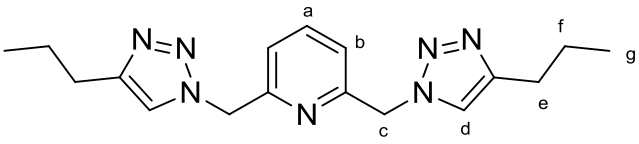

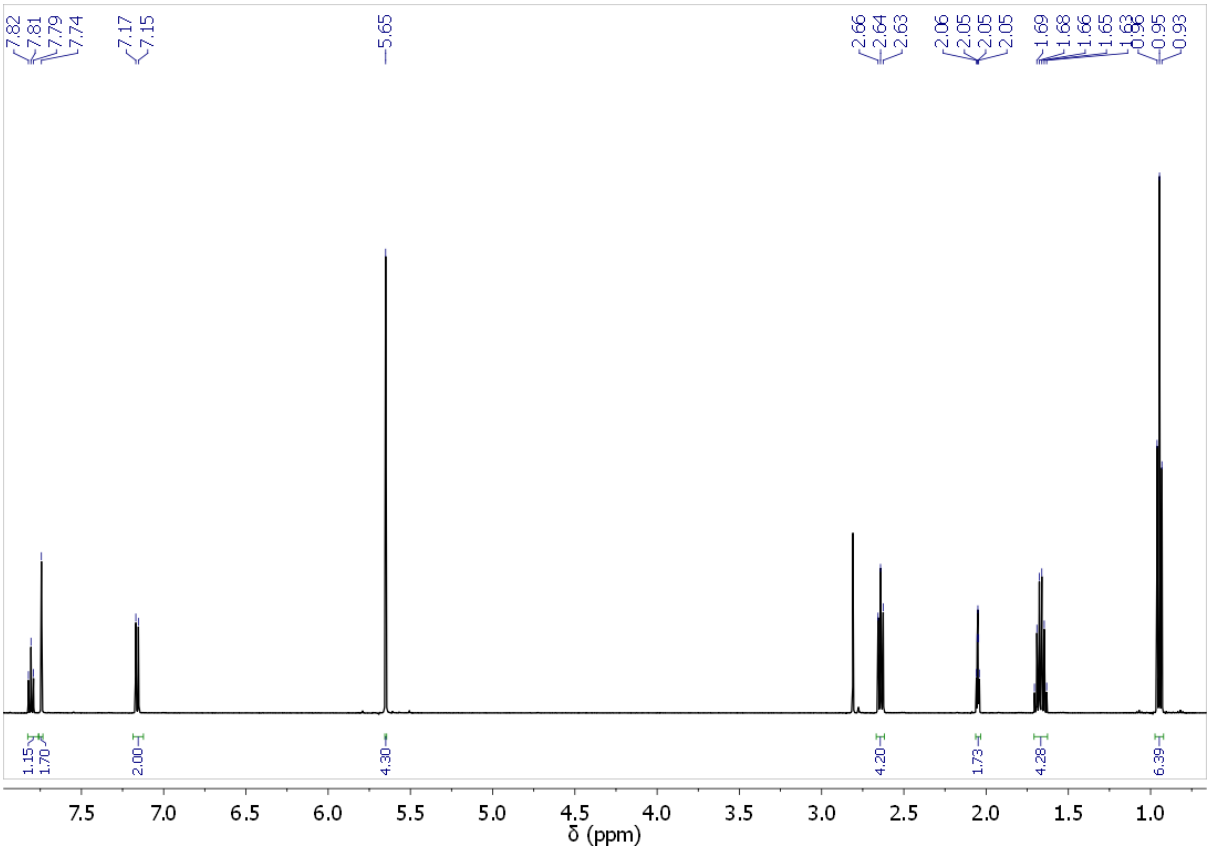

^{1}H NMR (d_6-acetone, 300K) of **3a.**

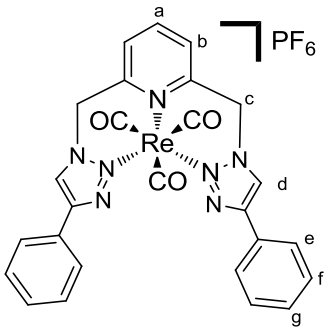

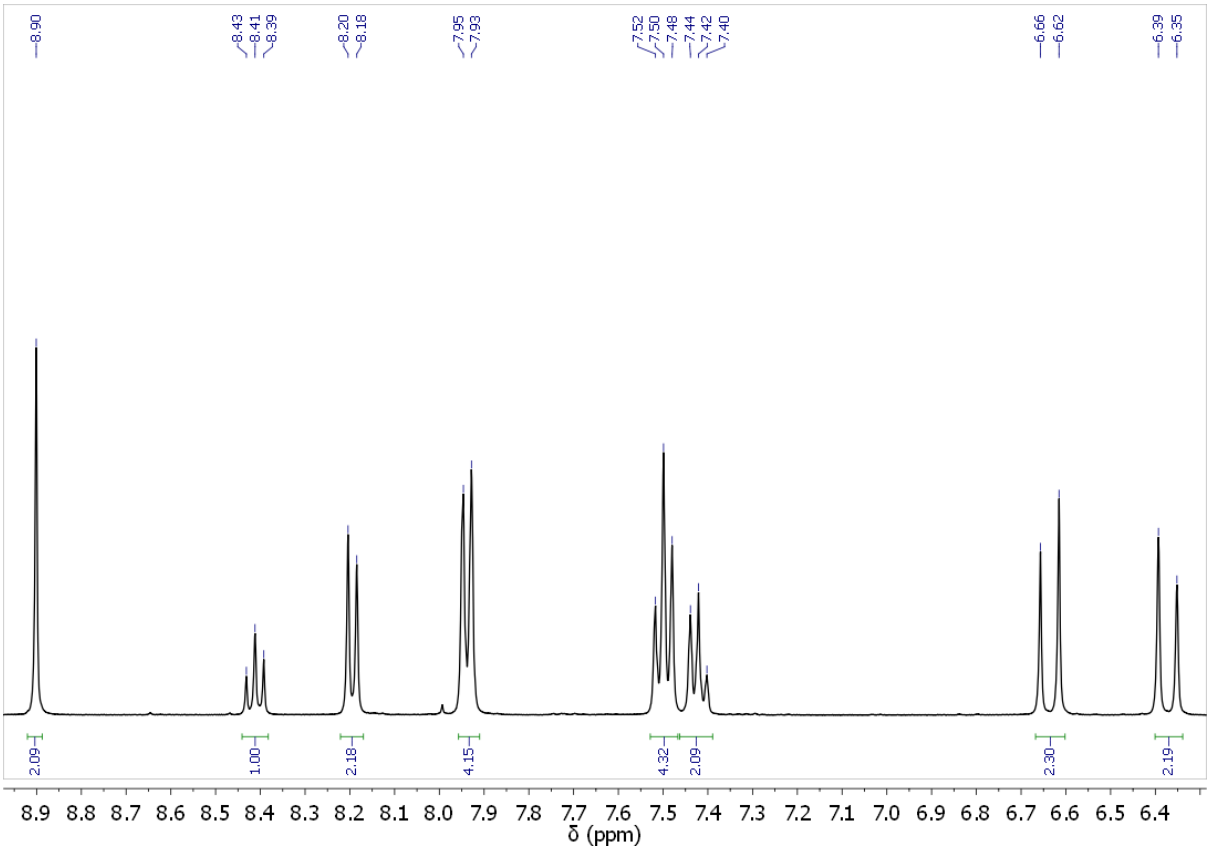

^{1}H NMR (d_6-acetone, 300K) of **3b.**

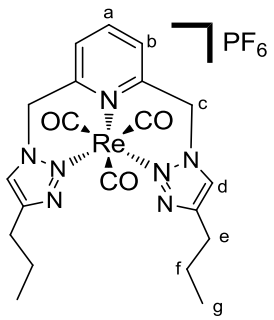

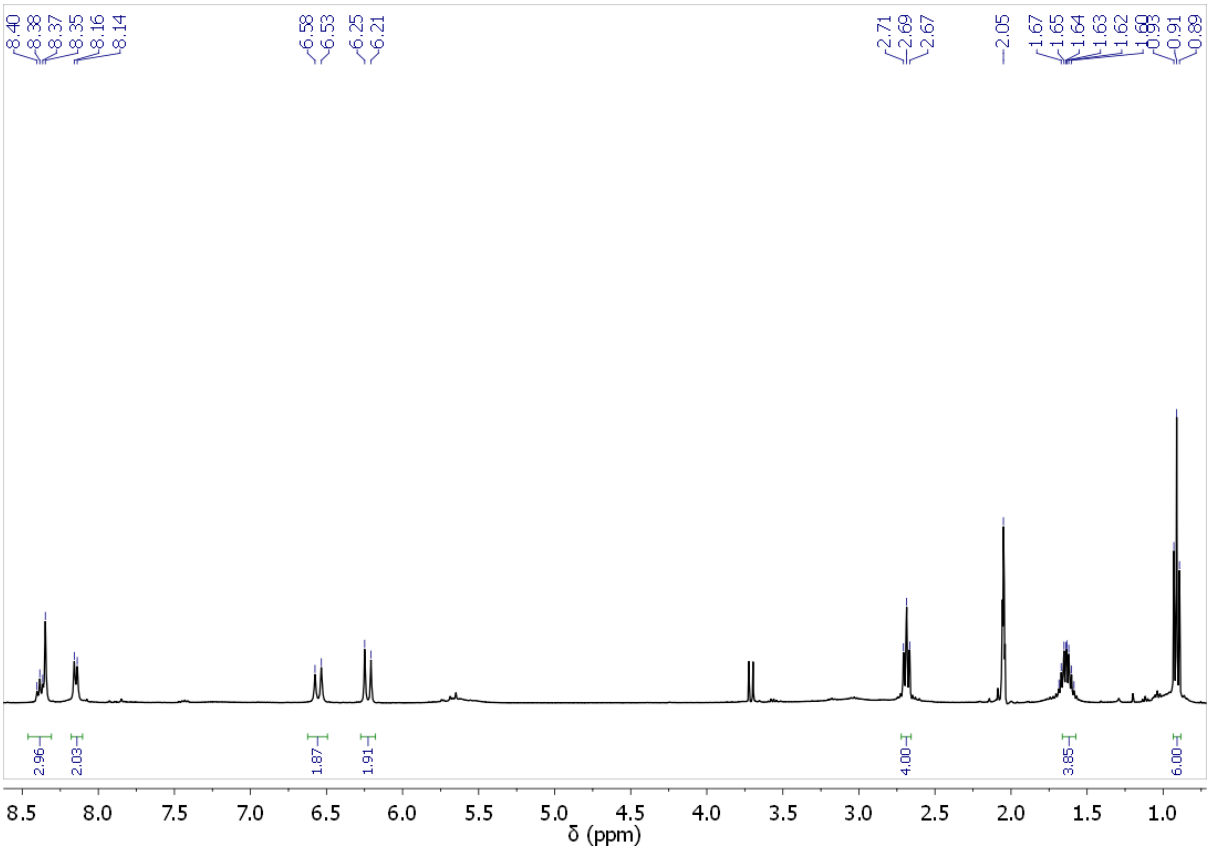

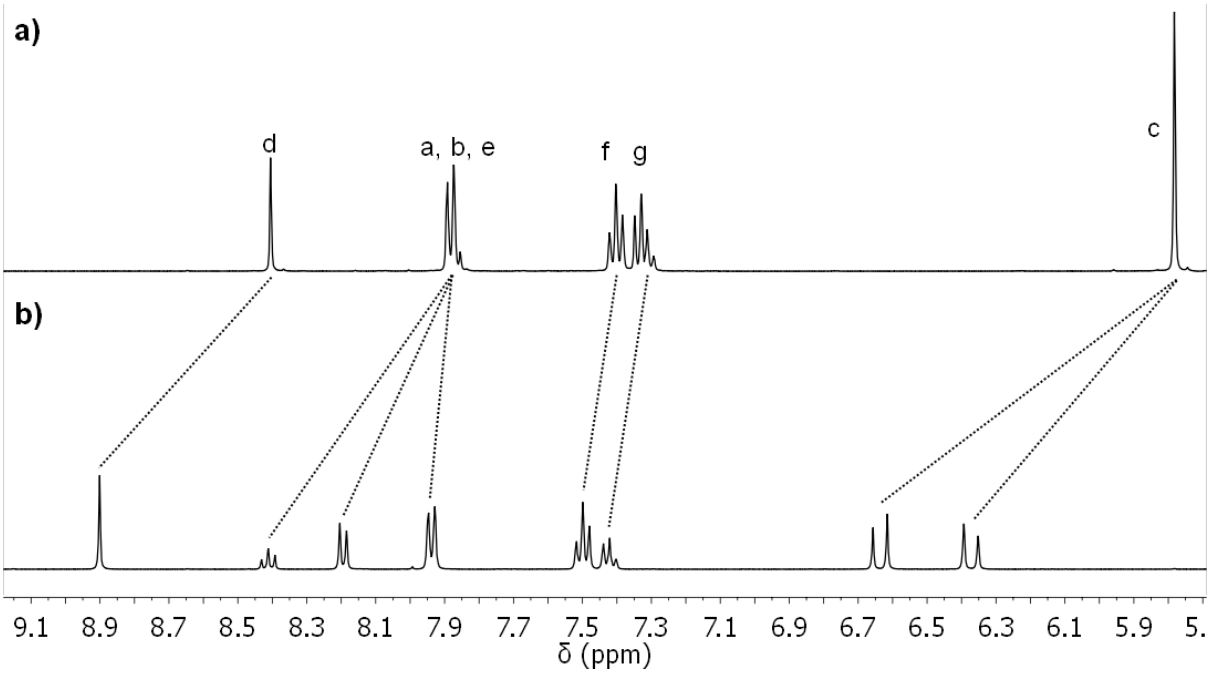

Figure S2-1 Partial ^{1}H NMR spectra (400 MHz, d_6-acetone, 298 K) of a) ligand **2a**, b) complex **3a**.

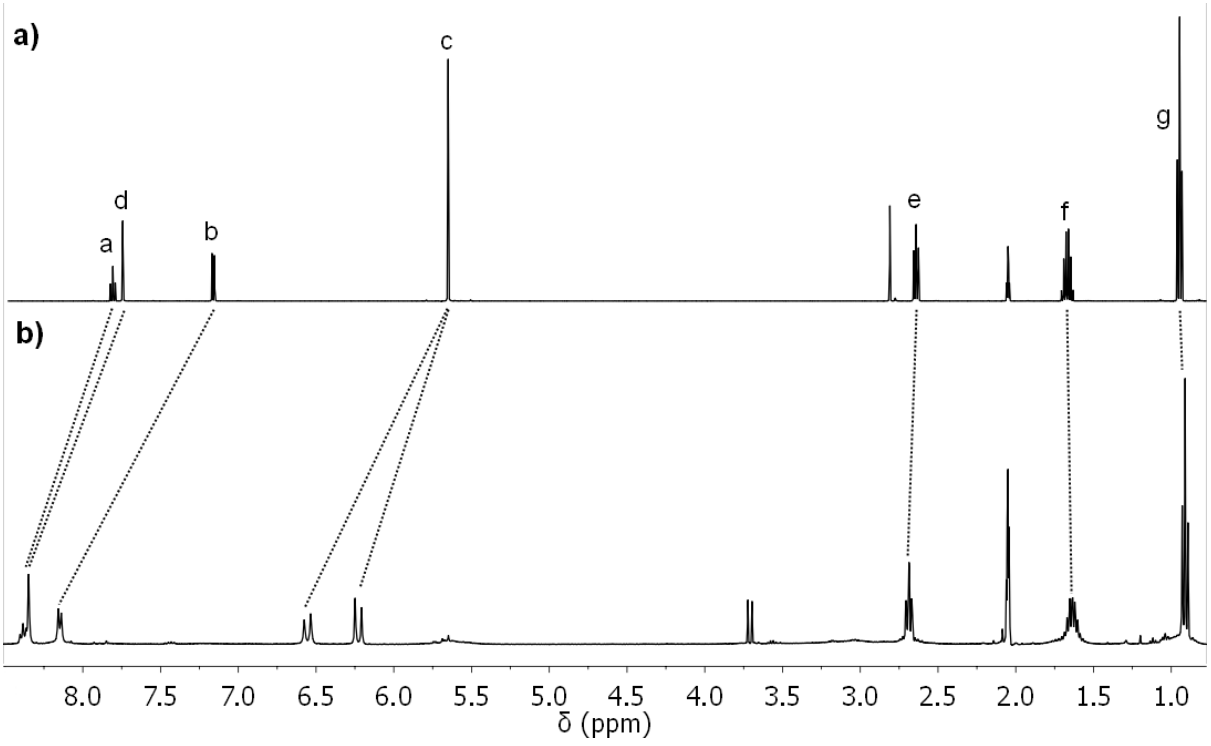

Figure S2-2 ^{1}H NMR spectra (400 MHz, d_6-acetone, 298 K) of a) Ligand **2b**, b) **3b**.

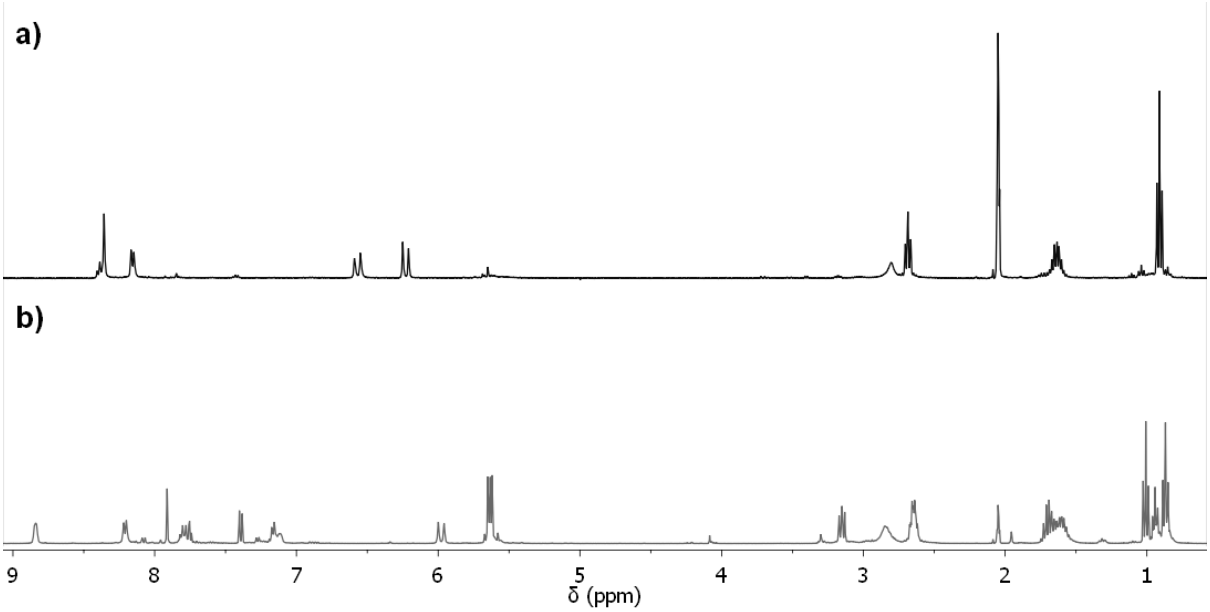

Figure S2-3 ^{1}H NMR spectra (400 MHz, d_6-acetone, 298 K) of a) complex **3b**, and b) the product of reaction when no $AgPF_6$ was used during the complexation.

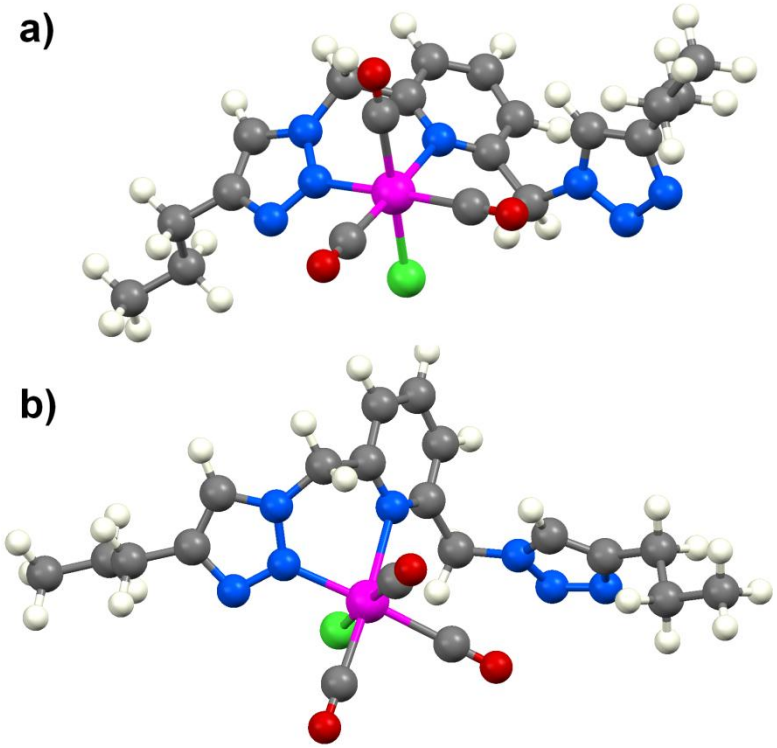

Figure S2-4 Spartan™ models of the proposed structure of the complexation of **2b** and $[Re(CO)_5Cl]$ without $AgPF_6$ to sequester the chloride.

3. HR-ESI-MS

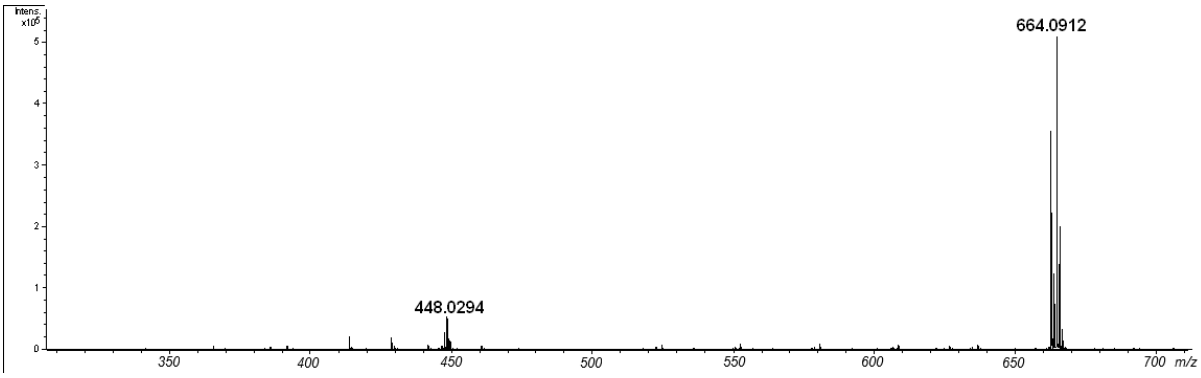

Figure S3-1 HS-ESI-MS showing the presence of [**3a** - PF_6]$^+$ and [**2a** +K]$^+$ in the mass spectroscopy experiments. (Isotopic distribution shown below)

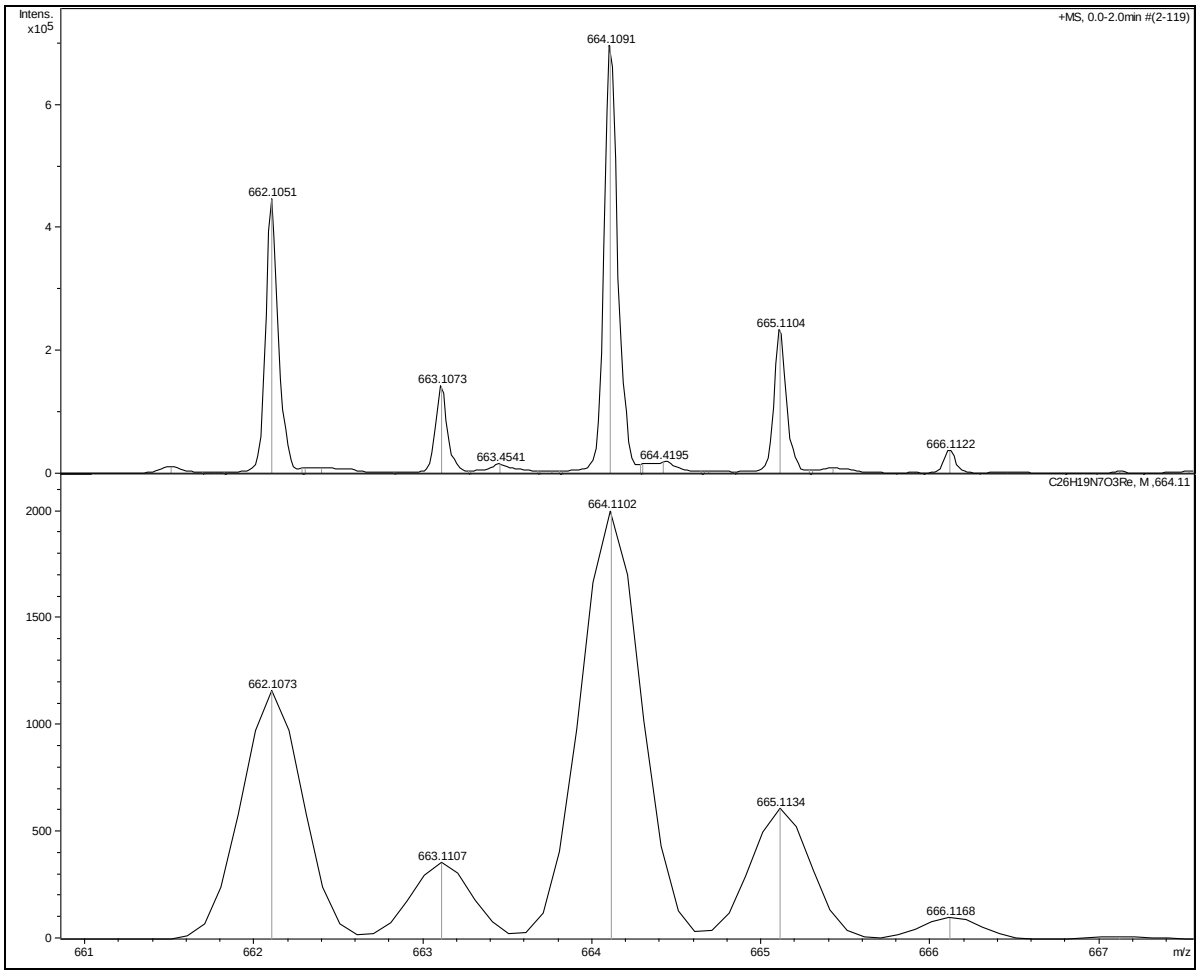

Figure S3-2 Observed (top) and calculated (bottom) isotopic distribution for the [**3a**-PF_6]$^+$ ion. Observed *m/z* 662.1051, 663.1073, 664.1091, 665.1104, 666.1122; calculated *m/z* 662.1073, 663.1107, 664.1102, 665.1134, 666.1168.

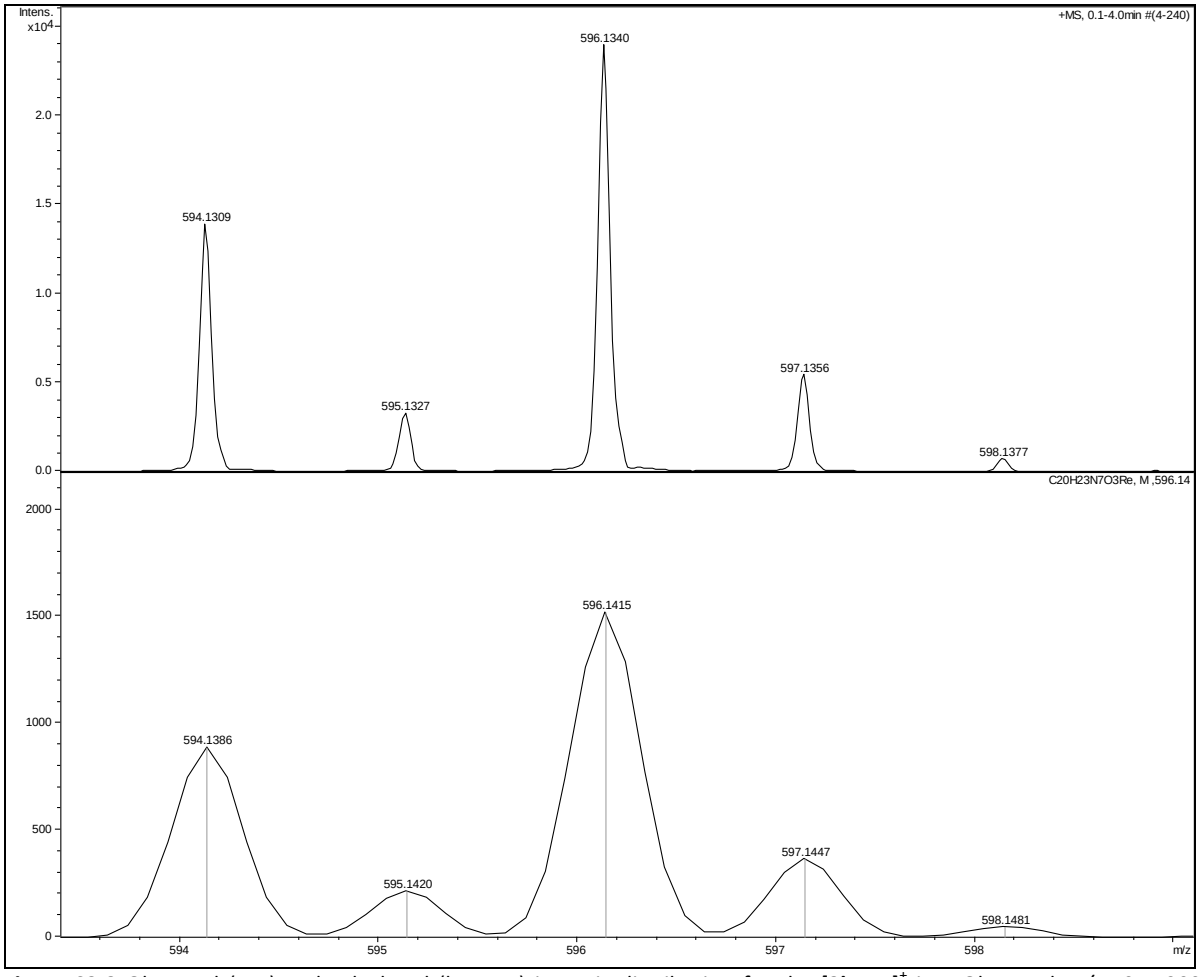

Figure S3-3 Observed (top) and calculated (bottom) isotopic distribution for the [**3b**-PF_6]$^+$ ion. Observed *m/z* 594.1309, 595.1327, 596.1340, 597.1656, 598.1377; calculated *m/z* 594.1386, 595.1420, 594.1415, 597.1447, 598.1481.

4. X-ray Crystallography

4.1 X-Ray Data Collection and Refinement

X-Ray data for **3a** and **3b** were recorded using a Bruker APEX II CCD diffractometer using Mo-Kα radiation (λ = 0.71073 Å). Full-matrix least-squares refinement on F^2 was carried out using SHELXL-97[1] with all non-hydrogen atoms being refined anisotropically. The hydrogen atoms were included in calculated positions and were refined as riding atoms with individual (or group, if appropriate) isotropic displacement parameters. In the case of **3b** two of the propyl arms (C_{15}, C_{16} & C_{17} and C_{51}, C_{52} & C_{53}) contained anisotropic ellipsoids that suggested certain atoms (C_{16}, C_{52} and C_{53}) could be split into two separate disordered parts. In the case of one of the arms (C_{17}, C_{16} & C_{15}) the terminal and pivotal carbon atoms (C_{17} and C_{15}) were ordered, with the central carbon atom (C_{16}) disordered over two sites. In the case of the other arm (C_{51}, C_{52} and C_{53}) the terminal carbon atom (C_{51}) was ordered with the remaining two carbon atoms each disordered over two sites. Despite modeling of this disorder resulting in more similar U_{eq} values for adjacent atoms, the bonding angles between the carbon atoms of the propyl arm do not form ideal tetrahedral geometries. Given the unequivocal identity of this moiety, attempts to restrain the data to give a more aesthetically pleasing model were deemed unnecessary. Although the hexafluorophosphate (PF_6-) anions were identified and attempts were made to model them, NPD atoms were observed. After attempts to impose restraints failed, SQUEEZE was used to eliminate the counterions and other diffuse disordered solvent molecules. See below for full SQUEEZE details. DELU command was used to restrain the anisotropic displacement parameters of the carbonyl atoms C_{22} and O_{22} to be more similar. The largest remaining residual density peak has a value of 4.205. This is located in a void space and is presumed to be residual density from diffuse solvent molecules that were located too close to the cationic portion of the structure to be affected by SQUEEZE. As such no serious attempts to model it were undertaken. The ORTEP[2] diagrams (Figure S3) have been drawn with 50% probability ellipsoids**.** Crystal data and collection parameters are given in Table S1. CCDC 885824 and 885825 contain the supplementary crystallographic data for **3a** and **3b** respectively. These data can be obtained free of

charge from the Cambridge Crystallographic Data Centre via www.ccdc.cam.ac.uk/data_request/cif

Table S1. Crystallographic Data

	3a	**3b**
CCDC Depository	885824	885825
Crystallization solvents	acetone/methanol	acetone/petrol
Empirical formula	$C_{26}H_{19}F_6N_7O_3PRe$	$C_{20}H_{23}F_6N_7O_3PRe$
Formula weight	808.65	741.62
T (K)	90(2)	89(2)
Crystal system	Monoclinic	Monoclinic
Space group	P2(1)/n	P2(1)/n
a (Å)	11.3982(10)	22.534(5)
b (Å)	13.1939(10)	10.528(2)
c (Å)	18.7735(15)	22.827(5)
α (°)	90	90
β (°)	99.246(3)	111.892(10)
γ (°)	90	90
V (Å^3)	2786.6	5025(2)
Z	4	8
ρ_{calc} (mg mm^{-3})	1.928	1.958
μ (mm^{-1})	4.502	4.983
Crystal size (mm)	0.4 x 0.2 x 0.2	0.47 x 0.46 x 0.21
Reflections collected	33919	128737
Independent reflections (R_{int})	5694 (0.1076)	10344 (0.0735)
Data/restraints/parameters	5186/0/397	10344/1/586
Goodness of fit	0.693	1.110
Final *R* indices[*I*>2σ(I)]	R1 = 0.0343, wR2 = 0.0882	R1 = 0.0382, wR2 = 0.1032
Final *R* indices (all data)	R1 = 0.0422, wR2 = 0.0960	R1 = 0.0469, wR2 = 0.1065
Largest diff. peak/hole	1.829 and -2.095	4.197 and -1.847

Table S4-1 Squeeze Results for **3b**

_platon_squeeze_void_nr	_platon_squeeze_void_average_x	_platon_squeeze_void_average_y	_platon_squeeze_void_average_z	_platon_squeeze_void_volume	_platon_squeeze_void_count_electrons
1	0.142	0.243	0.781	195.2	54.1
2	0.642	0.257	0.281	195.1	54.5
3	-0.142	0.757	0.219	195.2	55.3
4	0.358	0.743	0.719	195.2	56.2

Disordered hexafluorophosphate (PF_6^-) anions and disordered solvent molecules.

4.2 Molecular Diagrams.

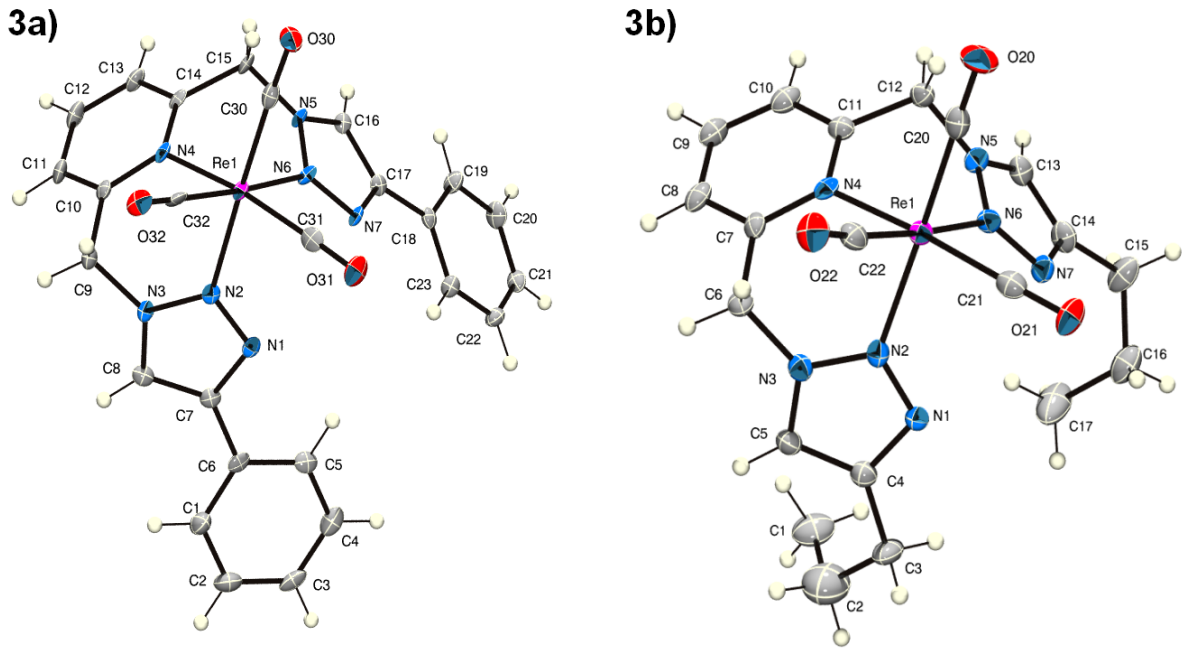

Figure S4-1 Labelled ORTEP diagrams of complexes **3a** and **3b**. Thermal ellipsoids are shown at the 50% probability level.

5. Emission Spectroscopy

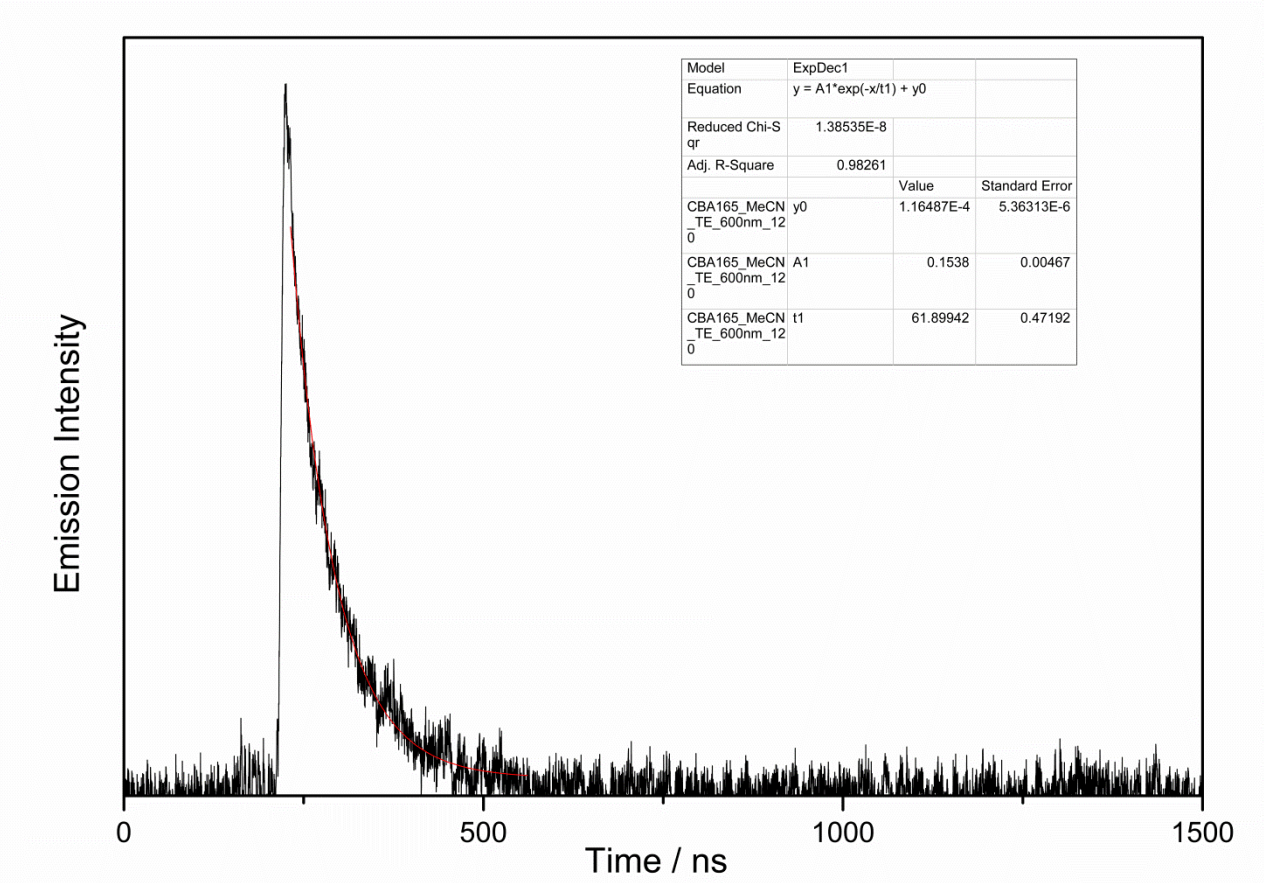

Figure S5-1 Fitted (red line) transient emission profile of **3a.**

6. Density Functional Theory Calculations

6.1 Method

In vacuo geometry optimisations, calculation of vibrational energy and electronic transitions were performed using density functional theory (DFT), employing the B3LYP functional.[3] A LAN2DZ pseudopotential was utilised to model the rhenium(I) ions with a 6-31G(d) basis set used on all remaining atoms. Geometries were first optimised without any symmetry constraints and the minima characterised via calculation of the vibrational energies. A result with no calculated negative energies ensures a global minimum has been established. Time-dependent DFT calculations of the optimised geometry at the CAM-B3LYP level of theory determined the simulated electronic absorption.

6.2 Calculated Geometry, Molecular Orbitals and Electronic Transitions

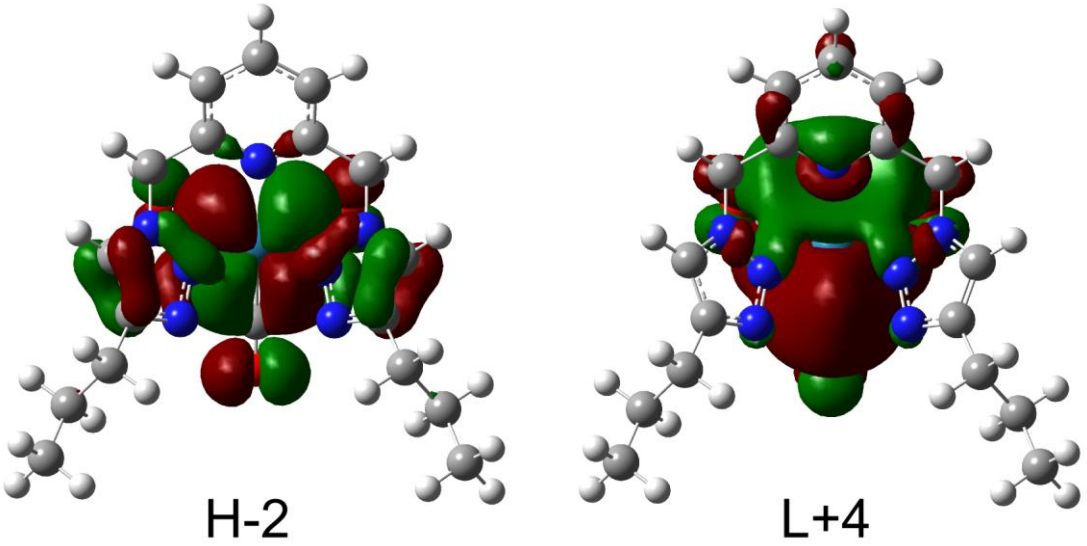

Figure S6-1 Diagrams of selected molecular orbitals of **3b** obtained from TD-DFT calculations.

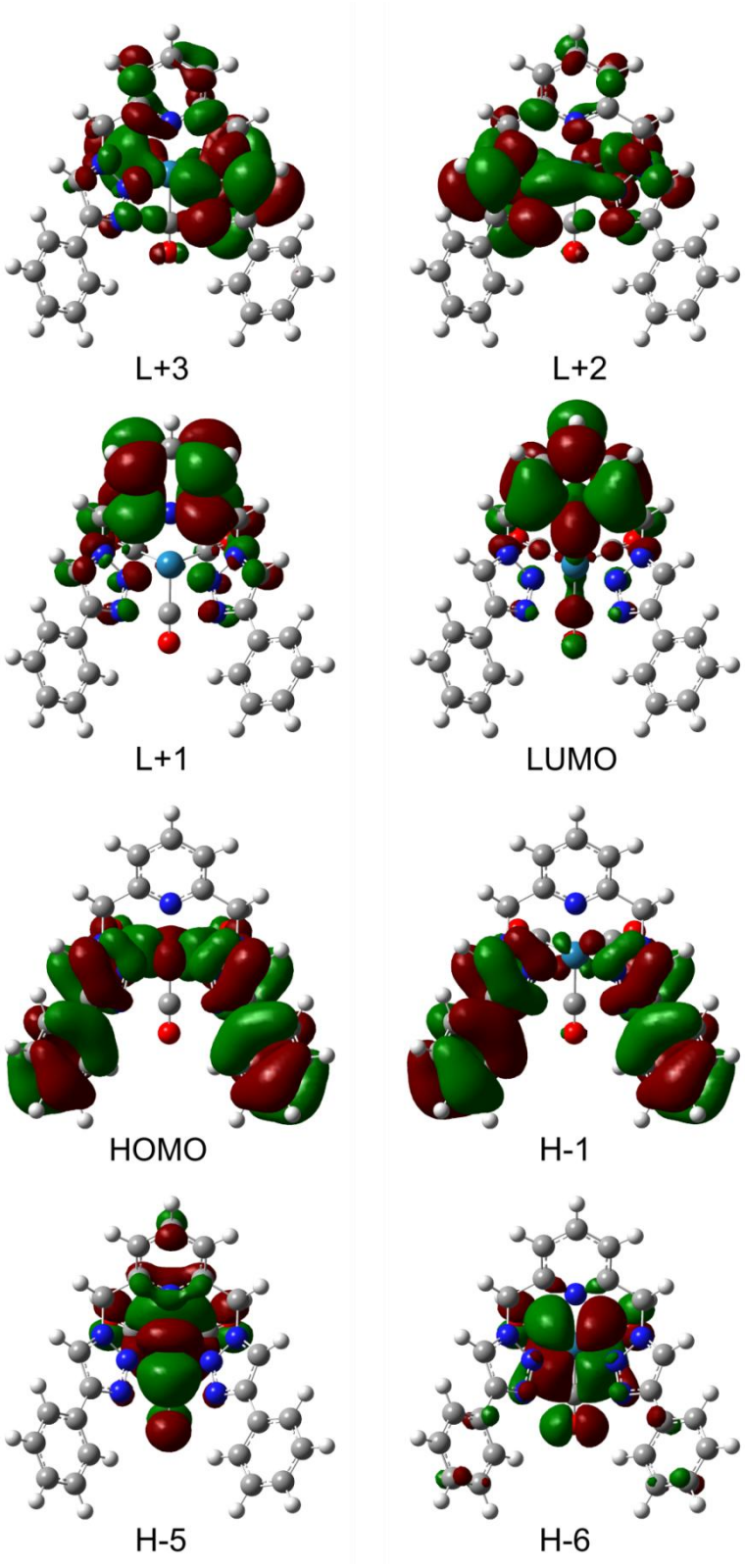

Figure S6-2 Diagrams of selected molecular orbitals of **3a** obtained from TD-DFT calculations.

7. References

(1) Sheldrick, G. M. *Acta Crystallogr., Sect. A: Found. Crystallogr.* **2008**, *A64*, 112-122.

(2) Farrugia, L. J. *J. Appl. Crystallogr.* **1997**, *30*, 565.

(3) Frisch, M. J.; Trucks, G. W.; Schlegel, H. B.; Scuseria, G. E.; Robb, M. A.; Cheeseman, J. R.; Scalmani, G.; Barone, V.; Mennucci, B.; Petersson, G. A.; Nakatsuji, H.; Caricato, M.; Li, X.; Hratchian, H. P.; Izmaylov, A. F.; Bloino, J.; Zheng, G.; Sonnenberg, J. L.; M. Hada, M. E.; Toyota, K.; Fukuda, R.; Hasegawa, J.; Ishida, M.; Nakajima, T.; Honda, Y.; Kitao, O.; Nakai, H.; Vreven, T.; J. A. Montgomery, J.; Peralta, J. E.; Ogliaro, F.; Bearpark, M.; Heyd, J. J.; Brothers, E.; Kudin, K. N.; Staroverov, V. N.; Kobayashi, R.; Normand, J.; Raghavachari, K.; Rendell, A.; Burant, J. C.; Iyengar, S. S.; Tomasi, J.; Cossi, M.; Rega, N.; Millam, J. M.; Klene, M.; Knox, J. E.; Cross, J. B.; Bakken, V.; Adamo, C.; Jaramillo, J.; Gomperts, R.; Stratmann, R. E.; Yazyev, O.; Austin, A. J.; Cammi, R.; Pomelli, C.; Ochterski, J. W.; Martin, R. L.; Morokuma, K.; Zakrzewski, V. G.; Voth, G. A.; Salvador, P.; Dannenberg, J. J.; Dapprich, S.; Daniels, A. D.; Farkas, Ö.; Foresman, J. B.; Ortiz, J. V.; Cioslowski, J.; D. J. Fox *Gaussian 09*; Gaussian, Inc.: Wallingford CT, 2009.